SI Appendix

V_H alignment

V_L alignment

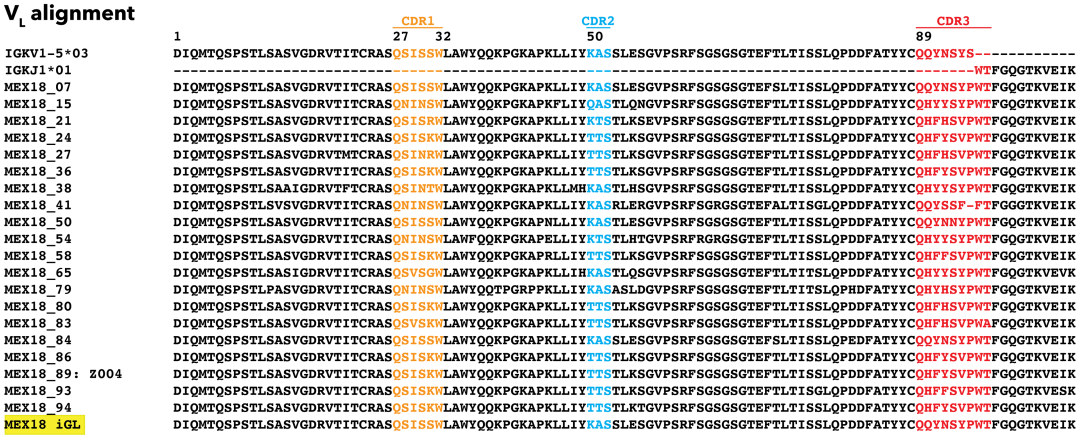

Figure S1. Alignments of V_H and V_L sequences of all 20 mature VH3-23/VK1-5 class Abs isolated from donor MEX 18 with their iGL (highlighted)[1]. The most common germline gene assignments (top lines) determined by IgBLAST for this set of Abs are shown[1]. For V_H, this includes the IGHV3-23*01 V gene segment, the IGHD3-10*01 D gene segment, and the IGHJ4*02 J gene segment. The D gene segment is shown as one possible reading frame. For V_L, this includes the IGKV1-5*03 V gene segment, and the IGKJ1*01 J gene segment. The mature Ab Z004 used for binding studies corresponds to the sequence MEX18_89. The Kabat numbering scheme was used.

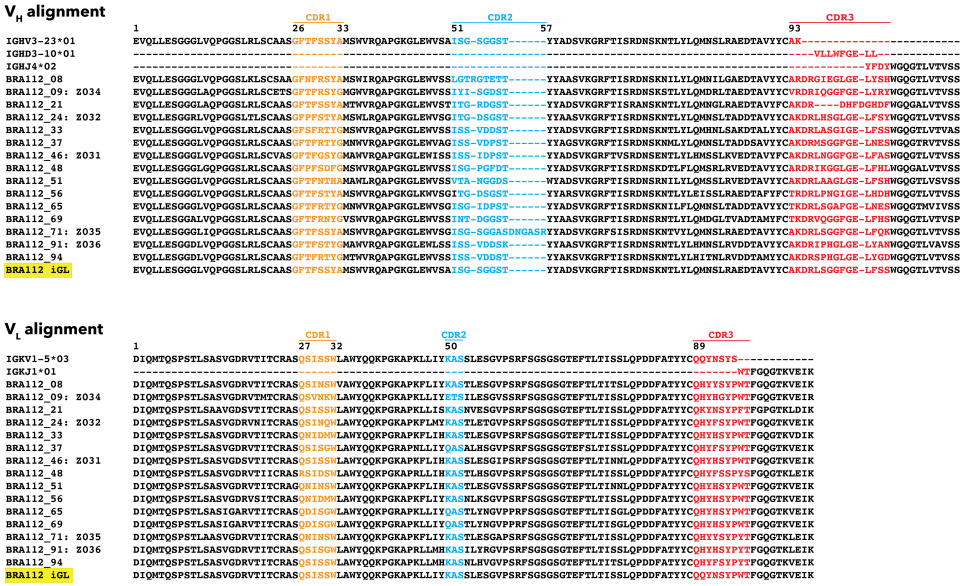

Figure S2. Alignments of V_H and V_L sequences of all 15 mature VH3-23/VK1-5 class Abs isolated from donor BRA 112 with their iGL (highlighted)[1]. The most common germline gene assignments (top lines) determined by IgBLAST for this set of Abs are shown[1]. For V_H, this includes the IGHV3-23*01 V gene, the IGHD3-10*01 D gene, and the IGHJ4*02 J gene. The D gene segment is shown as one possible reading frame. For V_L, this includes the IGKV1-5*03 V gene and IGKJ1*01 J gene. The Z03X mature Abs (Z034, Z032, Z031, Z035, and Z036) used for binding studies correspond to the sequences BRA112_09, BRA112_24, BRA112_46, BRA112_71, and BRA112_91 respectively. The Kabat numbering scheme was used.

V_H alignment

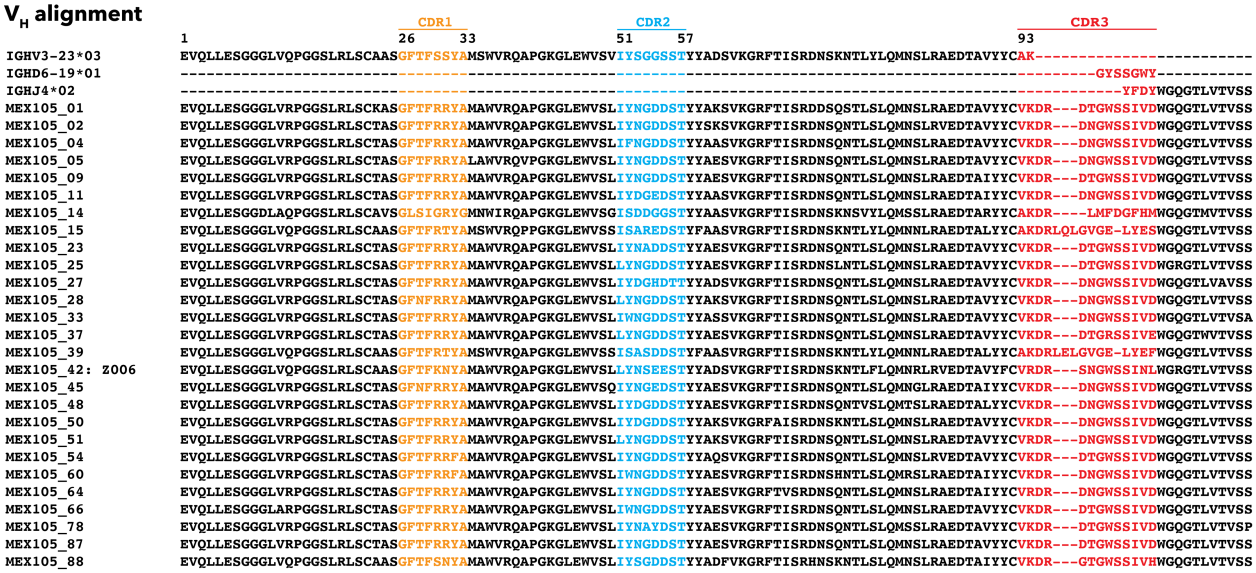

V_L alignment

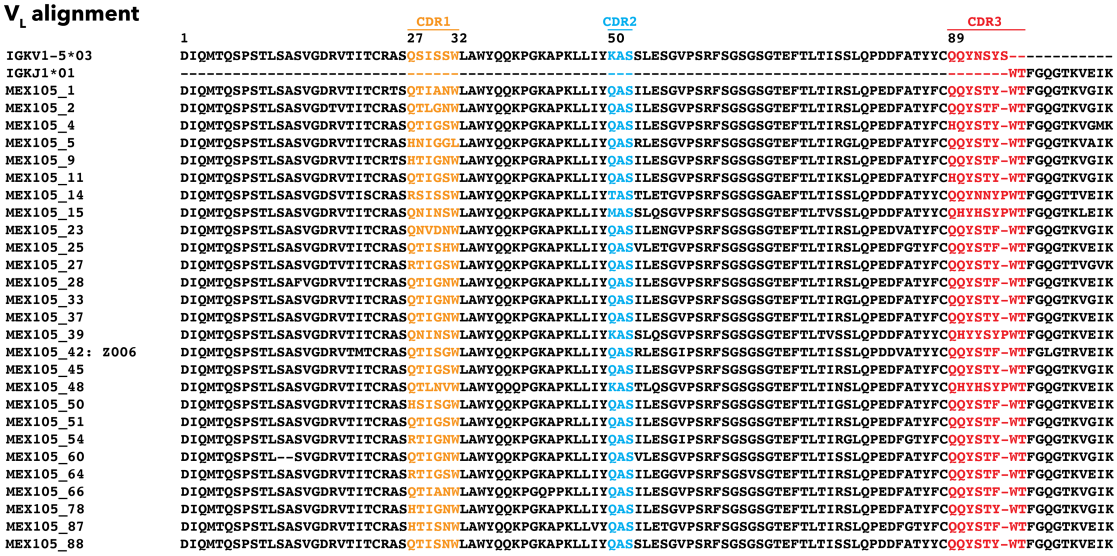

Figure S3. Alignments of V_H and V_L sequences of all 27 mature VH3-23/VK1-5 class Abs isolated from donor MEX 105 with CDRs highlighted[1]. The mature Ab Z006 used for binding studies corresponds to the sequence MEX105_42. The most common germline gene assignments (top lines) determined by IgBLAST for this set of Abs are shown[1]. For V_H, this includes the IGHV3-23*03 V gene segment, the IGHD6-19*01 D gene segment, and the IGHJ4*02 J gene segment. The D gene segment is shown as one possible reading frame. For V_L, this includes the IGKV1-5*03 V gene segment and the IGKJ1*01 J gene segment. The Kabat numbering scheme was used.

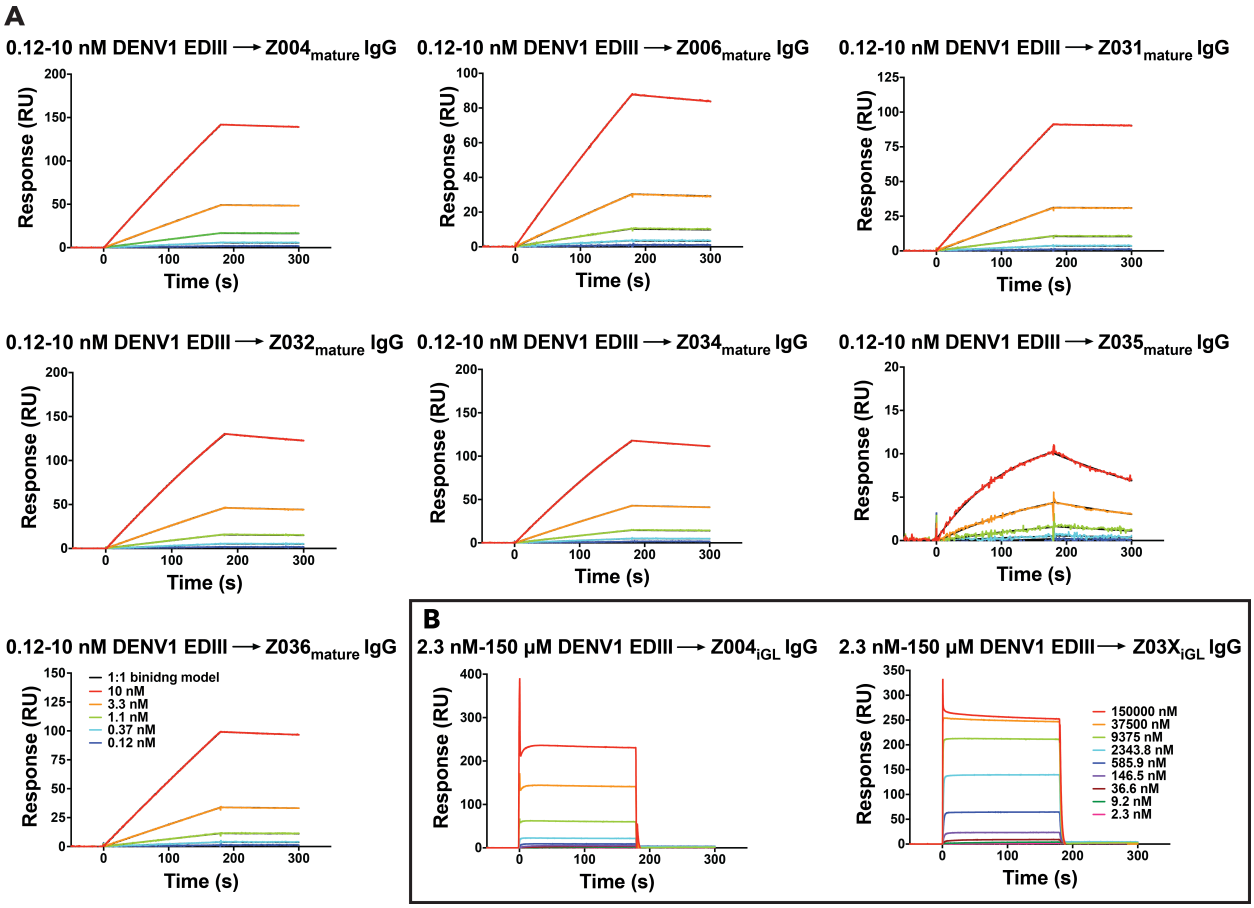

Figure S4. SPR binding assays with DENV1 EDIII. IgGs were captured on a protein A biosensor chip, and the indicated concentrations of DENV1 EDIII were injected. Sensorgrams are indicated in colors representing different injected concentrations. **A.** Mature IgGs binding to DENV1 EDIII. Fits to a 1:1 binding model are in black; since the models very closely fit the data, the models are only slightly visible. Residual plots for the 1:1 binding model fitting are shown in SI Appendix, Figure S7A. Two independent experiments were performed; the other set of sensorgrams is shown in Si Appendix, Figure S6. **B.** iGL IgGs binding to DENV1 EDIII. Fitting curves for equilibrium binding responses are shown in Figure 3. Y-axes show response units (RU).

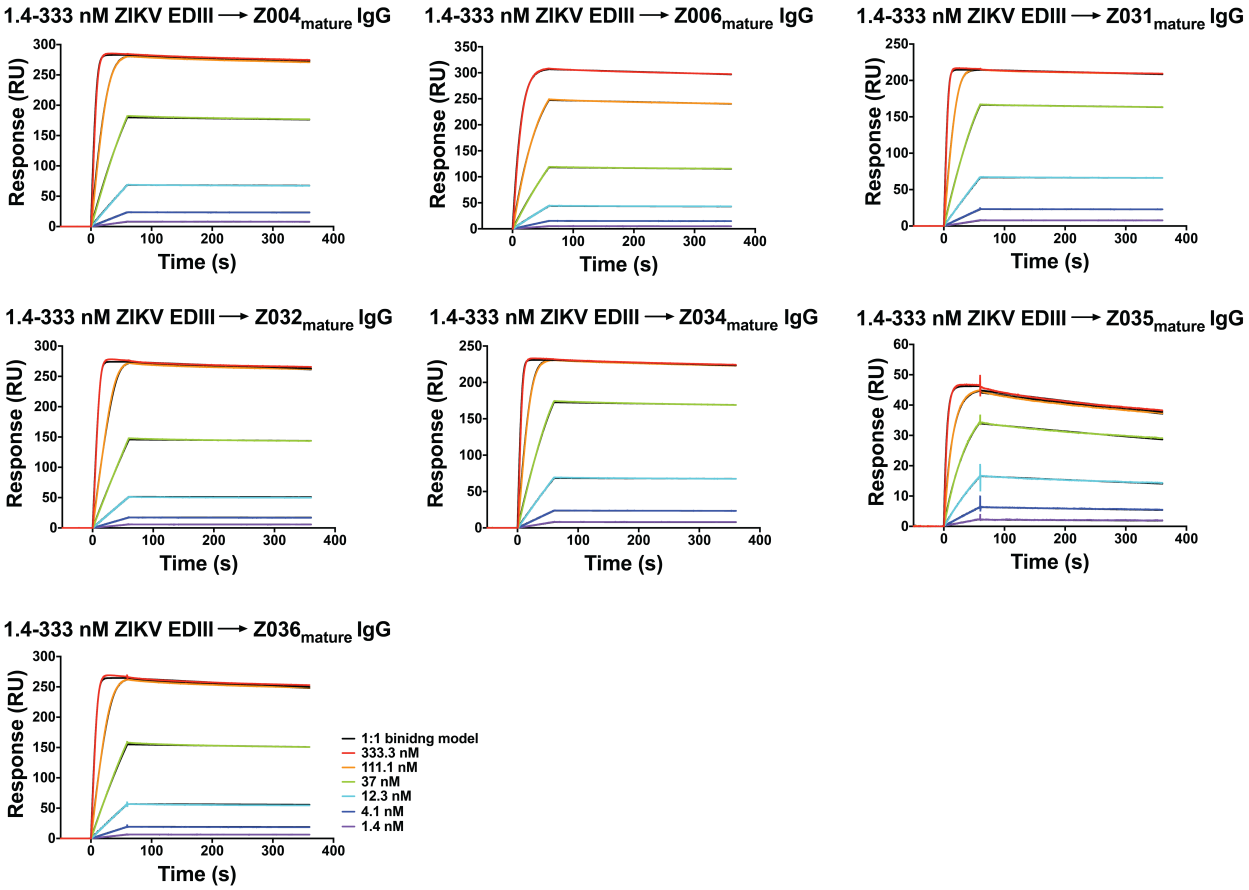

Figure S5. SPR binding assays with ZIKV EDIII. IgGs were captured on a protein A biosensor chip, and the indicated concentrations of ZIKV EDIII were injected. Sensorgrams are indicated in colors representing different injected concentrations. Mature IgGs binding to ZIKV EDIII. Fits to a 1:1 binding model are in black; since the models very closely fit the data, the models are only slightly visible. Residual plots for the 1:1 binding model fitting are shown in SI Appendix, Figure S7B. Y-axes show response units (RU). Two independent experiments were performed; the other set of sensorgrams is shown in Figure 2A.

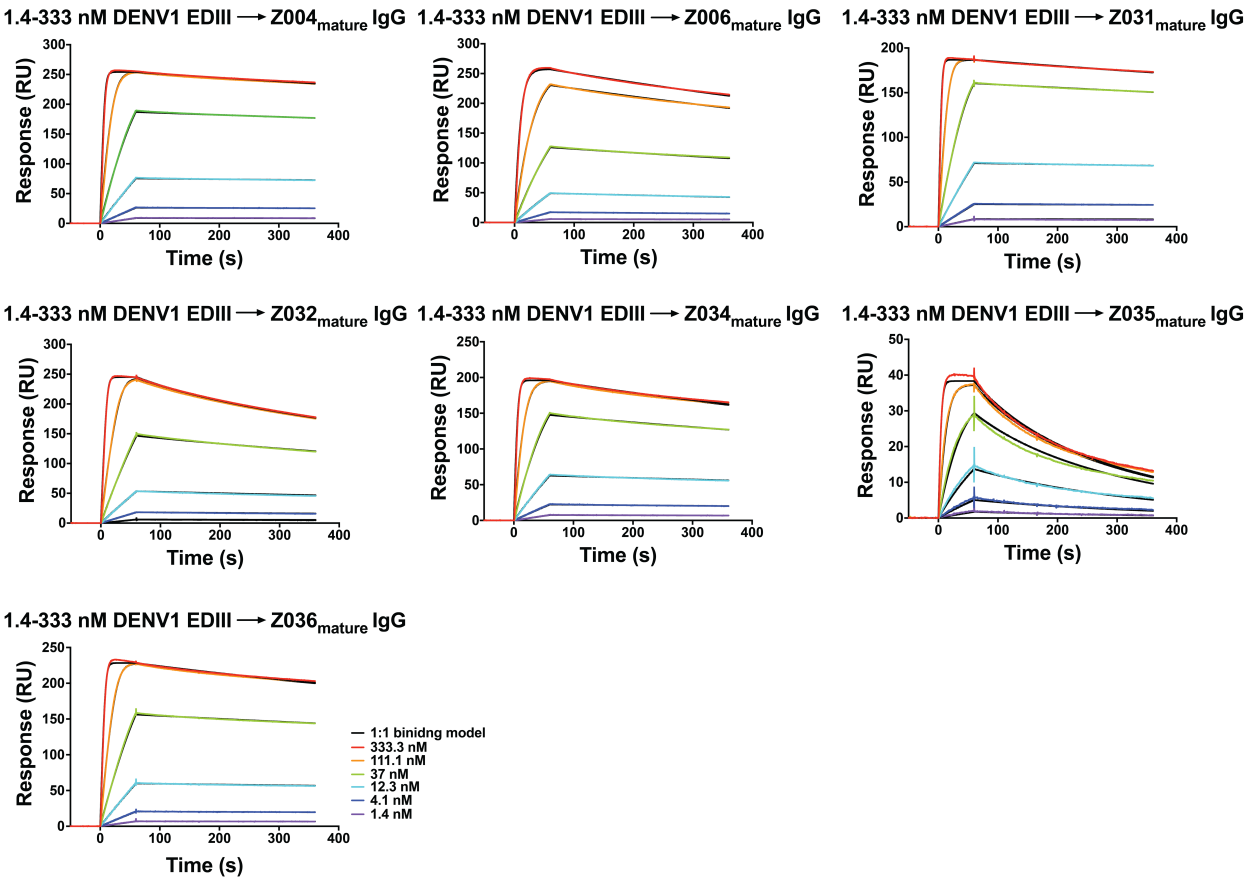

Figure S6. SPR binding assays with DENV1 EDIII. IgGs were captured on a protein A biosensor chip, and the indicated concentrations of DENV1 EDIII were injected. Sensorgrams are indicated in colors representing different injected concentrations. Mature IgGs binding to DENV1 EDIII. Fits to a 1:1 binding model are in black; since the models very closely fit the data, the models are only slightly visible. Residual plots for the 1:1 binding model fitting are shown in SI Appendix, Figure S7B. Y-axes show response units (RU). Two independent experiments were performed; the other set of sensorgrams is shown in SI Appendix, Figure S4A.

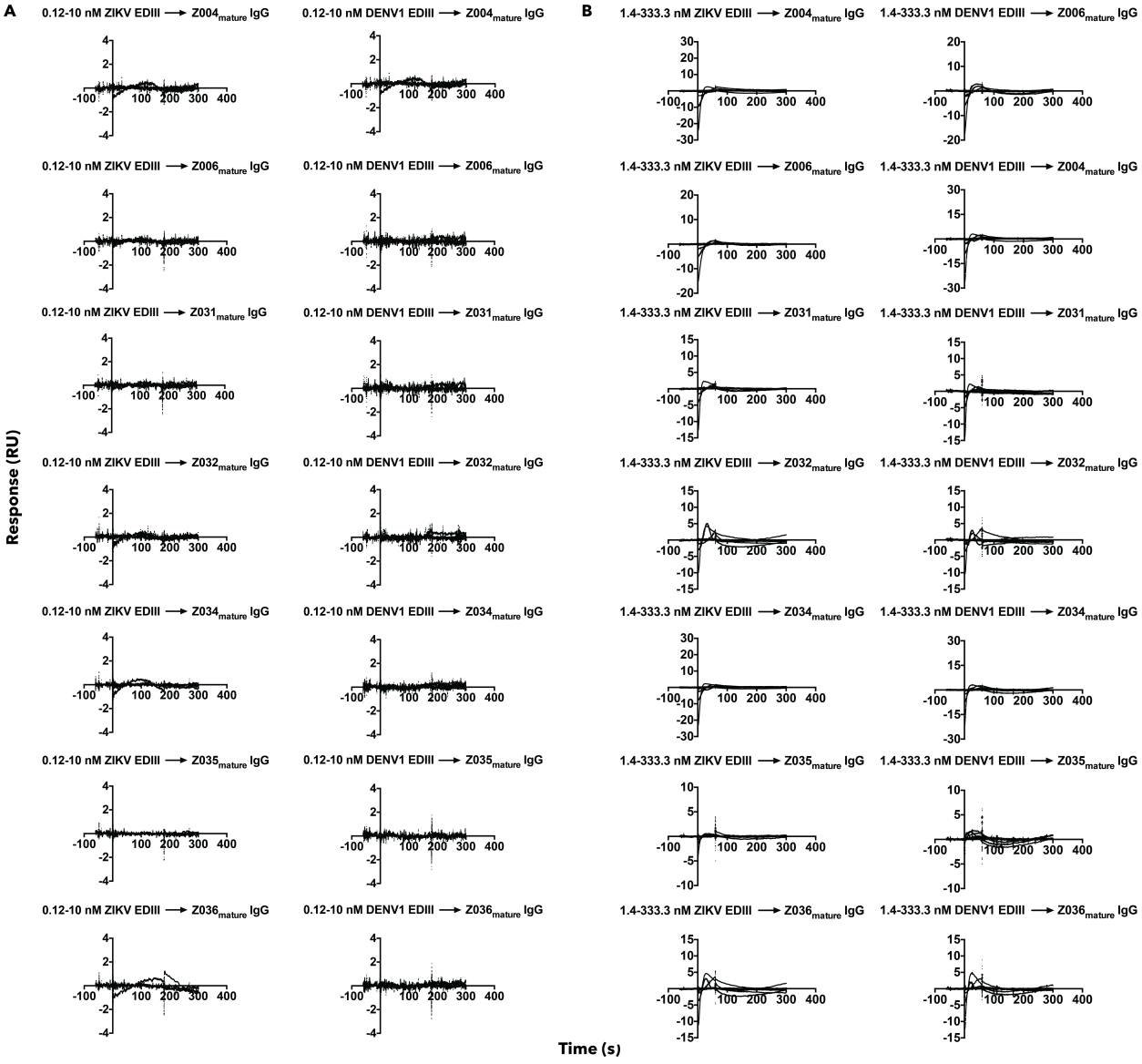

Figure S7. Residual plots for binding model fitting to SPR sensorgrams of ZIKV EDIII and DENV1 EDIII binding to mature IgGs from two independent experiments. **A.** Related to Figure 2A and SI Appendix, FigureS4A. **B.** Related to SI Appendix, Figures S5-S6. Y-axes shows response units (RU).

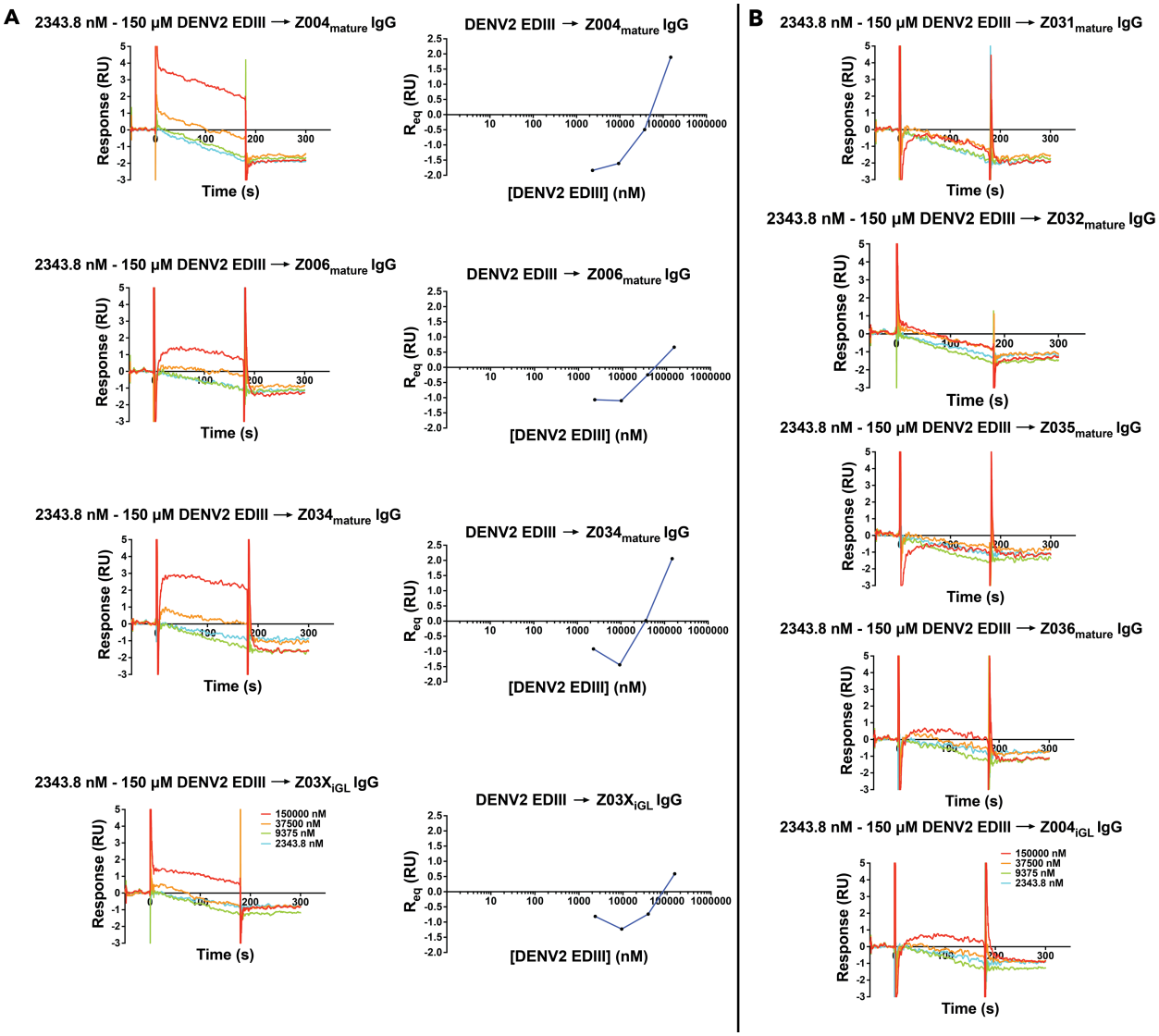

Figure S8. SPR binding assays for IgGs (ligands) interacting with DENV2 EDIII (analyte). IgGs were captured on a protein A biosensor chip, and the indicated concentrations of DENV2 EDIII were injected. Sensorgrams are indicated in colors representing different injected concentrations. **A.** Three mature IgG and one iGL IgG binding to DENV2 EDIII. Sensorgrams (left) and equilibrium binding curves (right) demonstrate weak binding of DENV2 EDIII to $Z004_{mature}$, $Z006_{mature}$, $Z034_{mature}$, and $Z03X_{iGL}$ IgGs. **B.** Four mature IgGs and one iGL IgG showed no binding to DENV2 EDIII. No detectable binding was found for $Z031_{mature}$, $Z032_{mature}$, $Z035_{mature}$, $Z036_{mature}$, and $Z004_{iGL}$ at concentrations ≤150 µM. Negative values indicate more DENV2 EDIII bound to the reference flow cell, HIV-1 IgG N6, than to the mature and iGL anti-ZIKV IgGs. Y-axes show response units (RU). Four independent injections were performed.

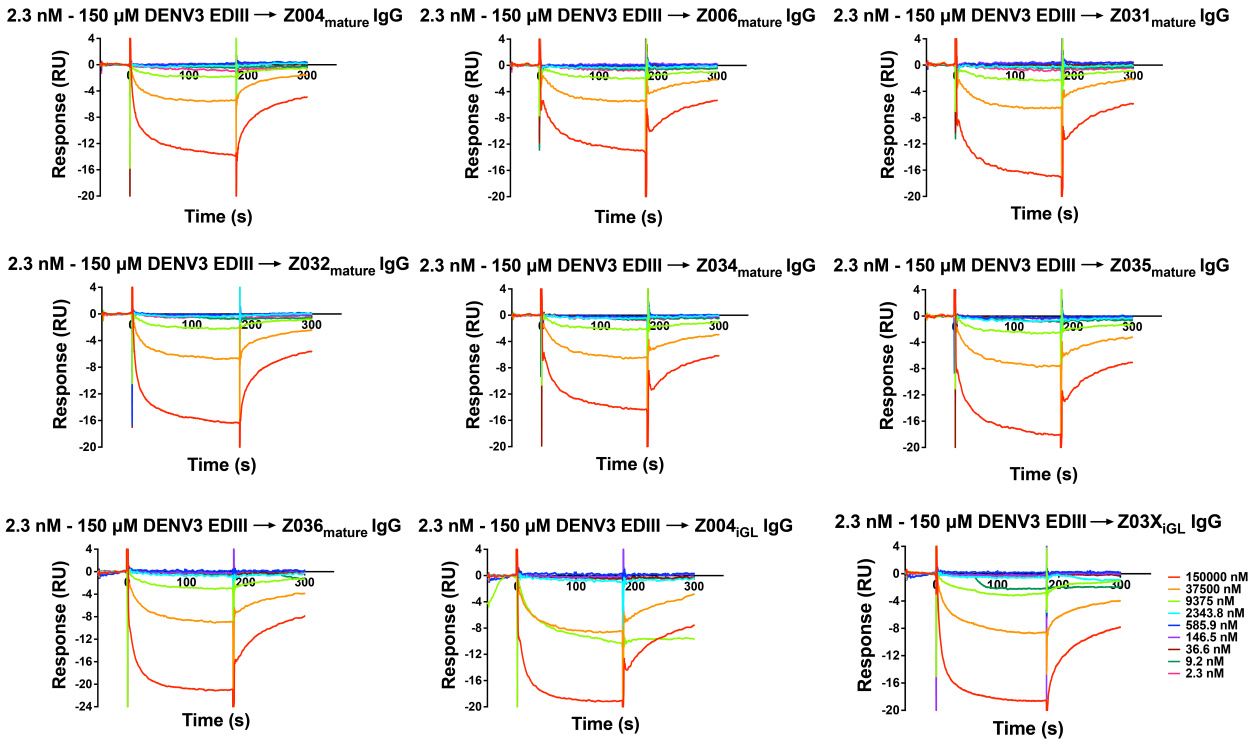

Figure S9. SPR binding assays for IgGs (ligands) interacting with DENV3 EDIII (analyte). IgGs were captured on a protein A biosensor chip, and the indicated concentrations of DENV3 EDIII were injected. Sensorgrams are indicated in colors representing different injected concentrations. No detectable binding was found for Z004$_{mature}$, Z006 $_{mature}$, Z031$_{mature}$, Z032 $_{mature}$, Z034 $_{mature}$, Z035 $_{mature}$, Z036 $_{mature}$, Z004$_{iGL}$, and Z03X$_{iGL}$ at concentrations ≤150 µM. Negative values indicate more DENV3 EDIII bound to the reference flow cell, HIV-1 IgG N6, than to the mature and iGL anti-ZIKV IgGs. Y-axes show response units (RU). Nine independent injections were performed.

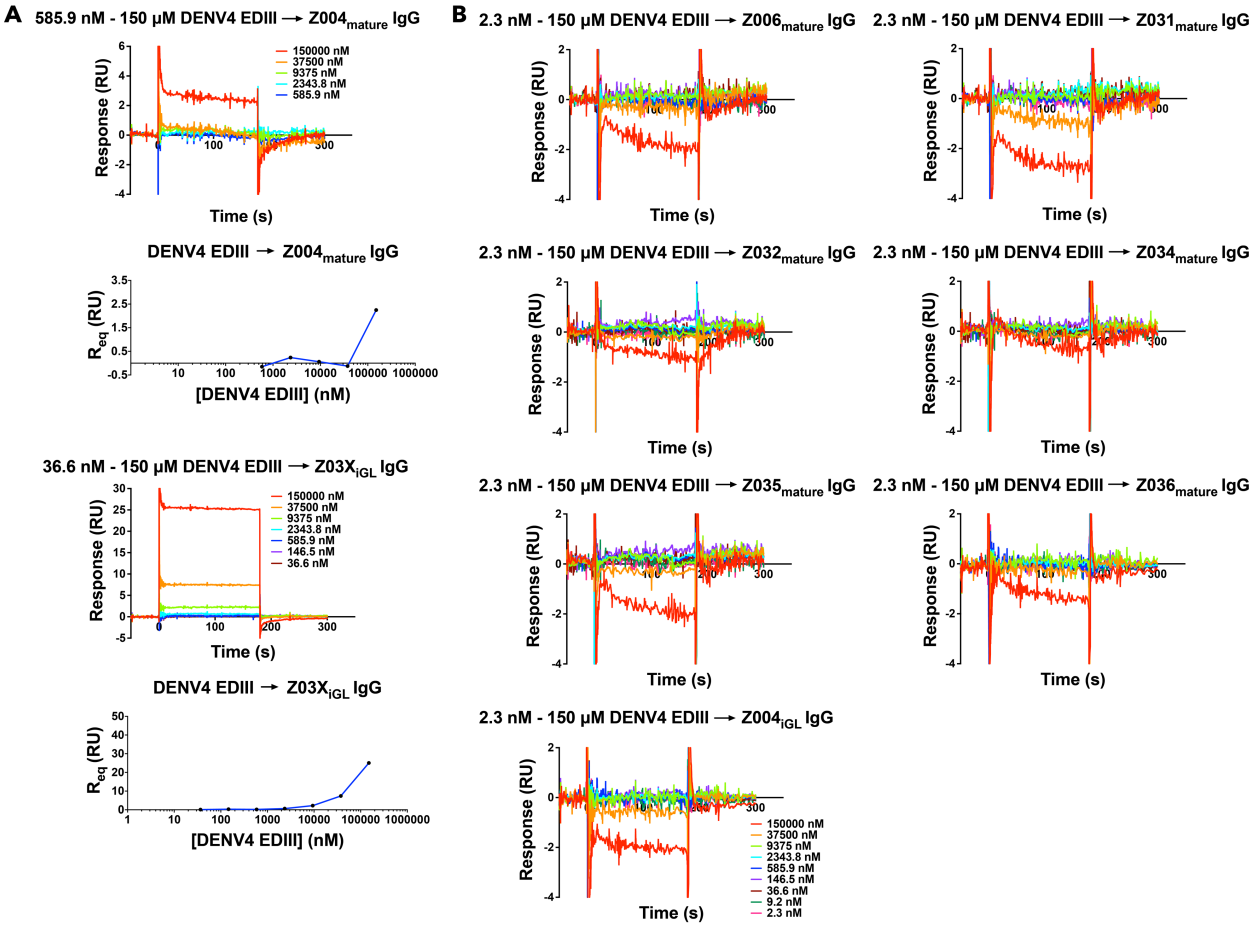

Figure S10. SPR binding assays for IgGs (ligands) interacting with DENV4 EDIII (analyte). IgGs were captured on a protein A biosensor chip, and the indicated concentrations of DENV4 EDIII were injected. Sensorgrams are indicated in colors representing different injected concentrations. **A.** One mature IgG and one iGL IgG binding to DENV4 EDIII. Sensorgrams (left) and equilibrium binding curves (right) demonstrate weak binding of DENV4 EDIII to $Z004_{mature}$ and $Z03X_{iGL}$ IgGs. **B.** Six mature IgGs and one iGL IgG showed no binding DENV4 EDIII. No detectable binding was found for $Z004_{mature}$, $Z006_{mature}$, $Z031_{mature}$, $Z032_{mature}$, $Z034_{mature}$, $Z035_{mature}$, $Z036_{mature}$, and $Z004_{iGL}$ at concentrations ≤150 µM. Negative values indicate more DENV4 EDIII bound to the reference flow cell, HIV-1 IgG N6, than to the mature and iGL anti-ZIKV IgGs. Y-axes show response units (RU). Five to nine independent injections were performed.

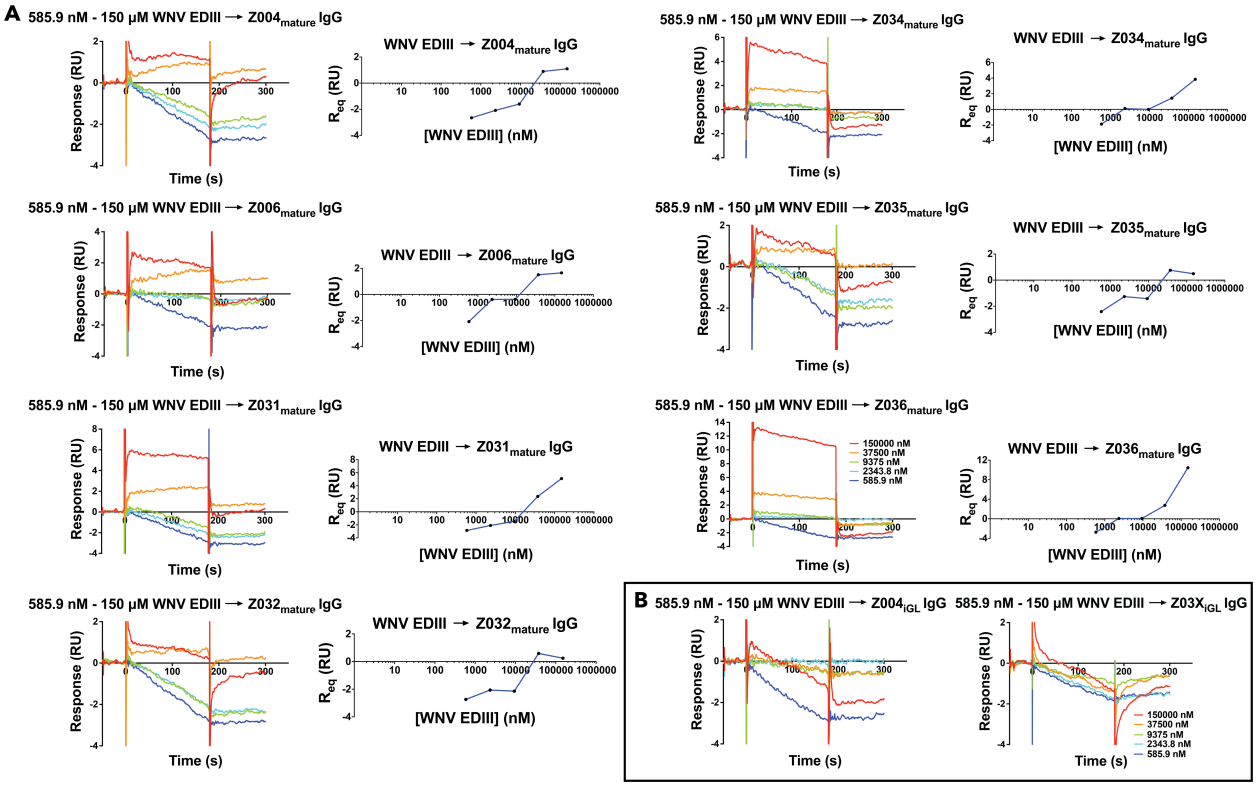

Figure S11. SPR binding assays for IgGs (ligands) interacting with WNV EDIII (analyte). IgGs were captured on a protein A biosensor chip, and the indicated concentrations of WNV EDIII were injected. Sensorgrams are indicated in colors representing different injected concentrations. **A.** Mature IgGs binding to WNV EDIII. Sensograms (left) and equilibrium binding curves (right) demonstrate weak binding of WNV EDIII to $Z004_{mature}$, $Z006_{mature}$, $Z031_{mature}$, $Z032_{mature}$, $Z034_{mature}$, $Z035_{mature}$, and $Z036_{mature}$. **B.** No detectable binding was found for $Z004_{iGL}$ and $Z03X_{iGL}$ at concentrations ≤150 μM. Negative values indicate more WNV EDIII bound to the reference flow cell, HIV-1 IgG N6, than to the mature and iGL anti-ZIKV IgGs. Y-axes show response units (RU). Five independent injections were performed.

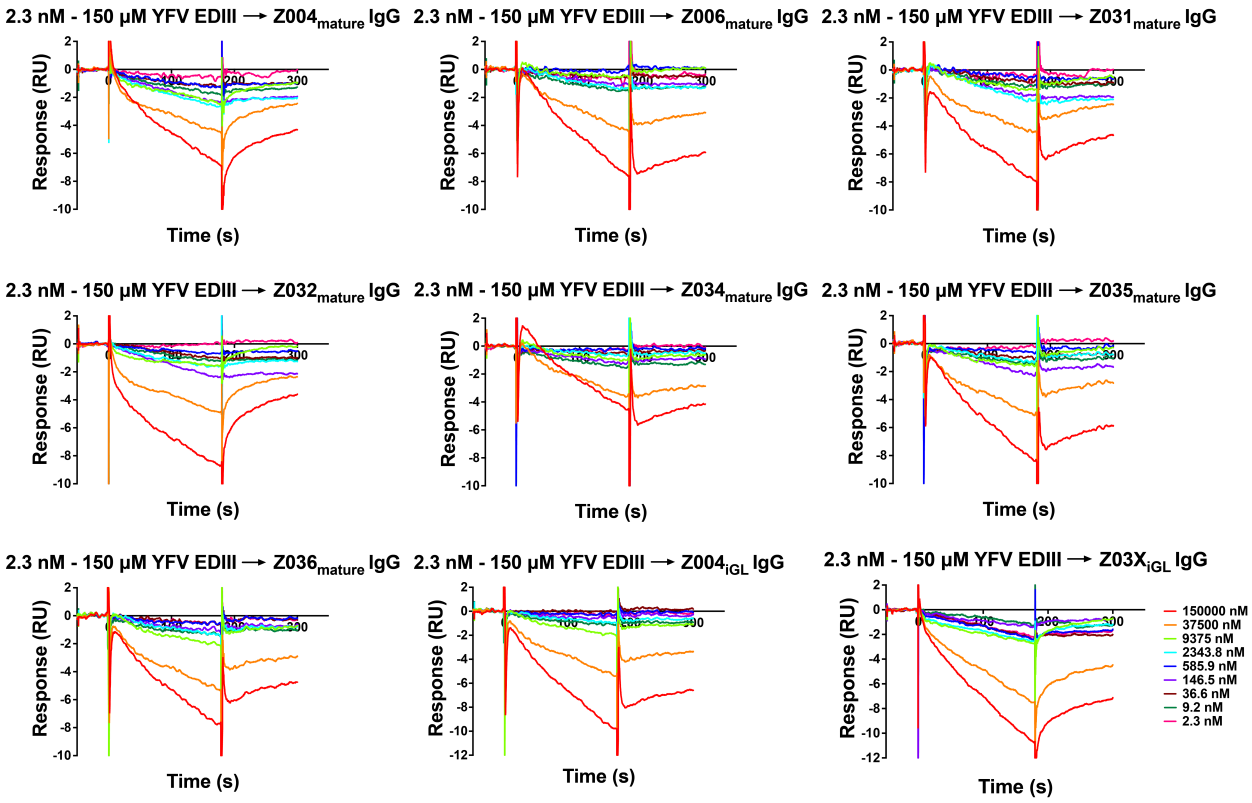

Figure S12. SPR binding assays for mature and iGL IgG (ligands) interacting with YFV EDIII (analyte). IgGs were captured on a protein A biosensor chip, and the indicated concentrations of YFV EDIII were injected. Sensorgrams are indicated in colors representing different injected concentrations. No detectable binding was found for any IgGs at YFV EDIII concentrations ≤150 µM. Note that negative values indicate more YFV EDIII binds to the reference flow cell, HIV-1 IgG N6, than to the mature and iGL anti-ZIKV IgGs. Y-axes show response units (RU). Nine independent injections were performed.

A

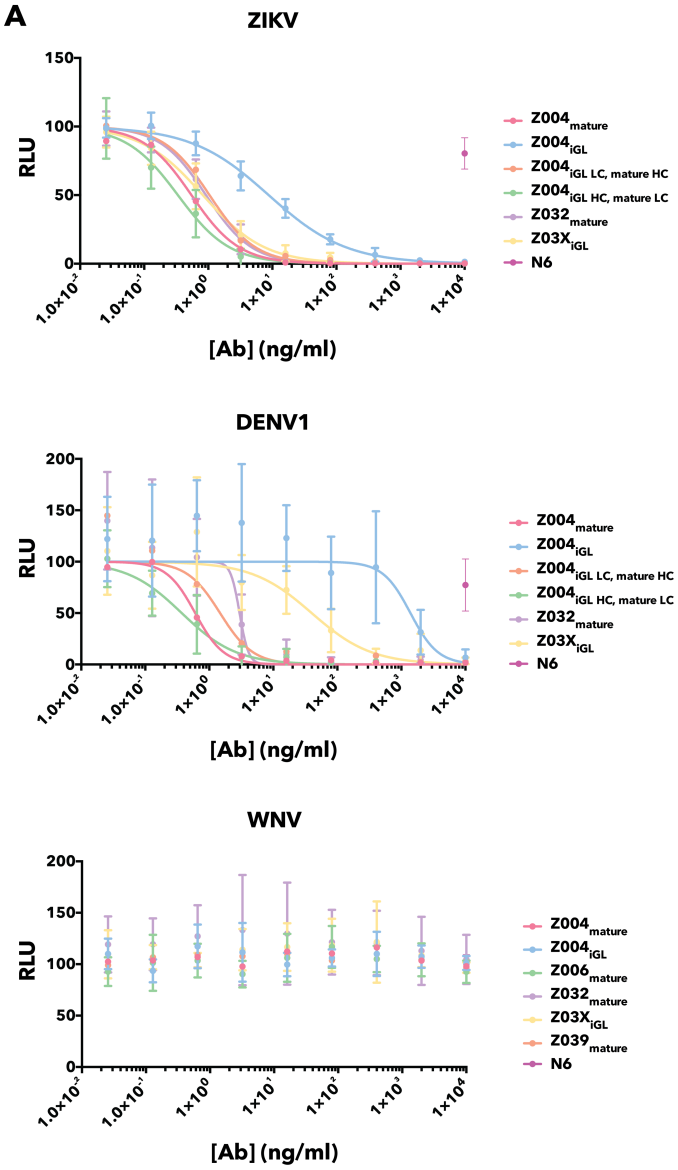

B

	ZIKV	DENV1
IgG	NT50 (ng/ml)	
$Z004_{mature}$	0.55	0.60
$Z004_{iGL}$	8.8	1400
$Z004_{iGL\ LC,\ mature\ HC}$	1.0	1.5
$Z004_{iGL\ HC,\ mature\ LC}$	0.34	0.37
$Z032_{mature}$	0.92	3.0
$Z03X_{iGL}$	0.82	40

Figure S13. RVP-based neutralization assays. **A.** Neutralization curves for Abs against ZIKV, DENV1 and WNV RVPs. Two or three independent experiments were performed and are plotted on the same graph. Y-axes show luciferase activity (relative light units, RLUs) normalized to RVP luciferase activity without Ab present. The HIV-1 Ab N6 (negative control) was assessed at the highest concentration (10 μg/ml). **B**. NT50s for Abs against ZIKV and DENV1 RVPs.

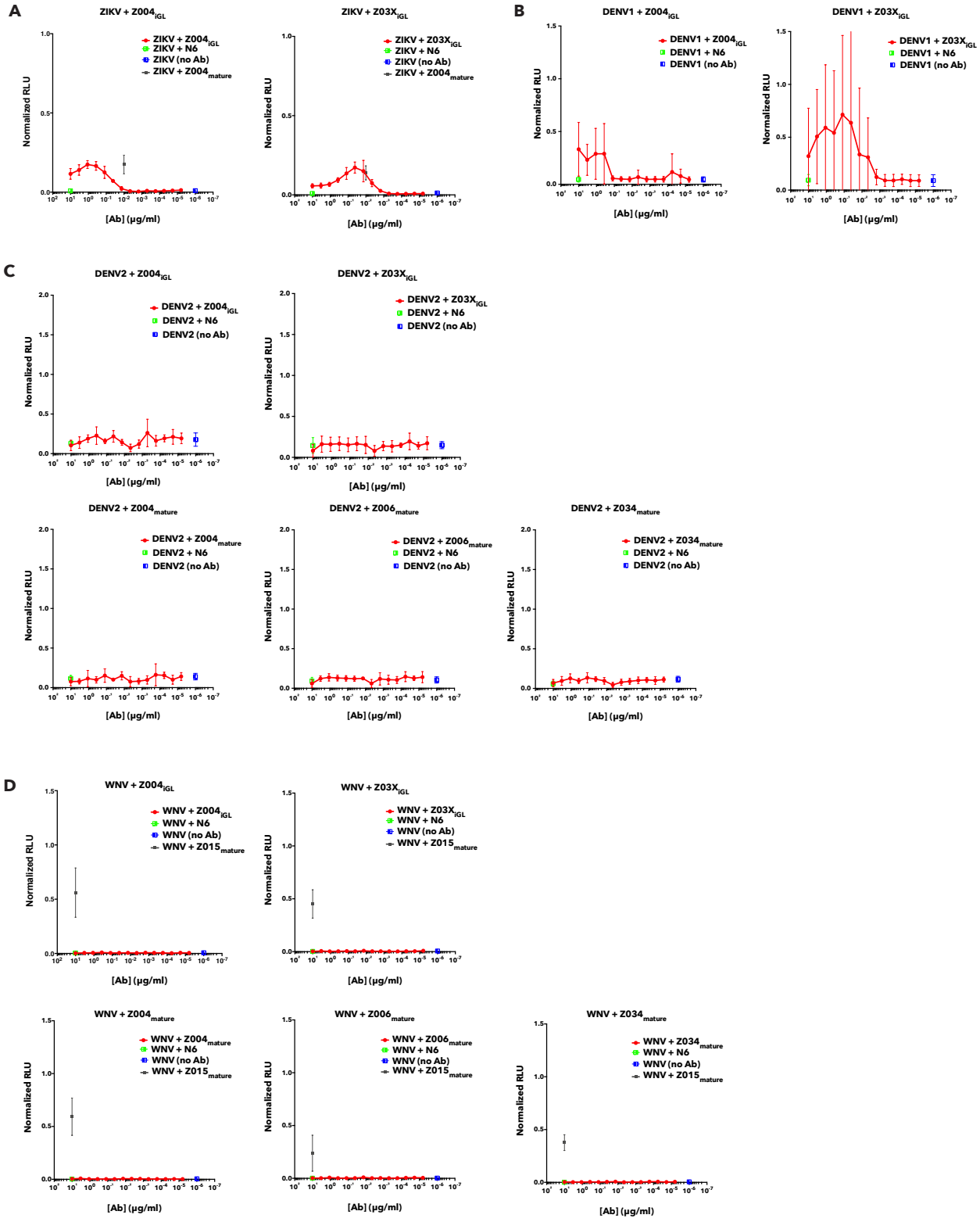

Figure S14. RVP-based ADE assays for Abs against **A.** ZIKV, **B.** DENV1, **C.** DENV2, and **D.** WNV RVPs. Two independent experiments were performed and the normalized data were combined. Data plotted is the luciferase activity (relative light units, RLUs) normalized to respective RVP luciferase activity determined on fully permissive Huh-7.5 cells (positive

control). The HIV-1 Ab N6 (negative control) and cross-reactive Ab $Z015_{mature}$ (WNV positive control) were assessed at the highest concentration (10 µg/ml). $Z004_{mature}$ Ab (ZIKV positive control) was assessed at 0.01 µg/ml, a concentration known to show ADE for ZIKV.

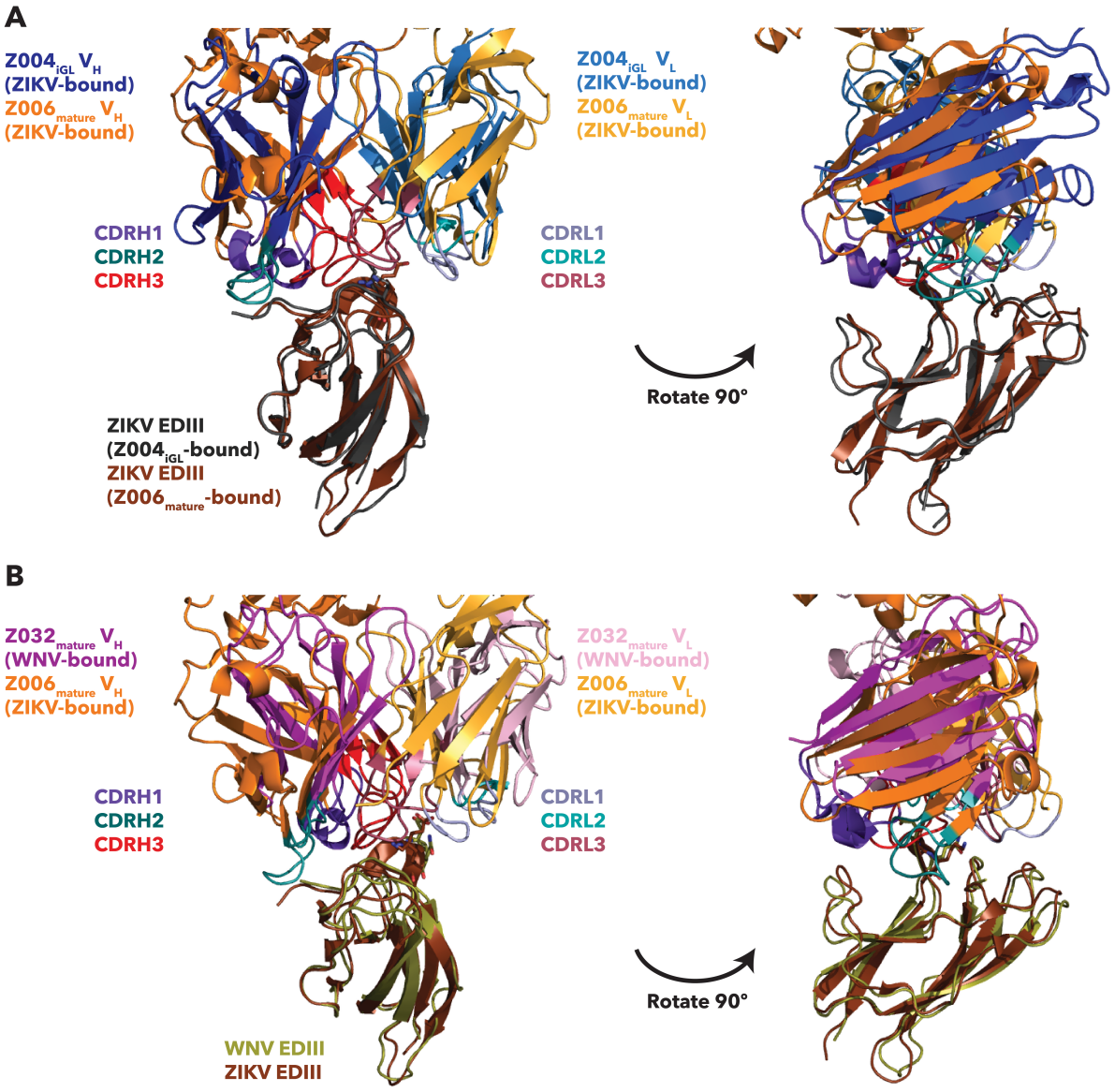

Figure S15. Recognition of EDIIIs by mature and iGL Fabs. Fab V_H-V_L-EDIII structures are shown as cartoon representations. The Fab C_H-C_L domains were truncated in the figure in order to focus on the V_H-V_L interaction with EDIII. Structures were superimposed on the EDIII. The ZIKV EK and WNV EQ motifs are shown as sticks. **A.** Superimposition of $Z004_{iGL}$ V_HV_L–ZIKV EDIII (Figure 4A) and $Z006_{mature}$–ZIKV EDIII structures. **B.** Superimposition of $Z006_{mature}$–ZIKV EDIII and $Z032_{mature}$–WNV EDIII structures.

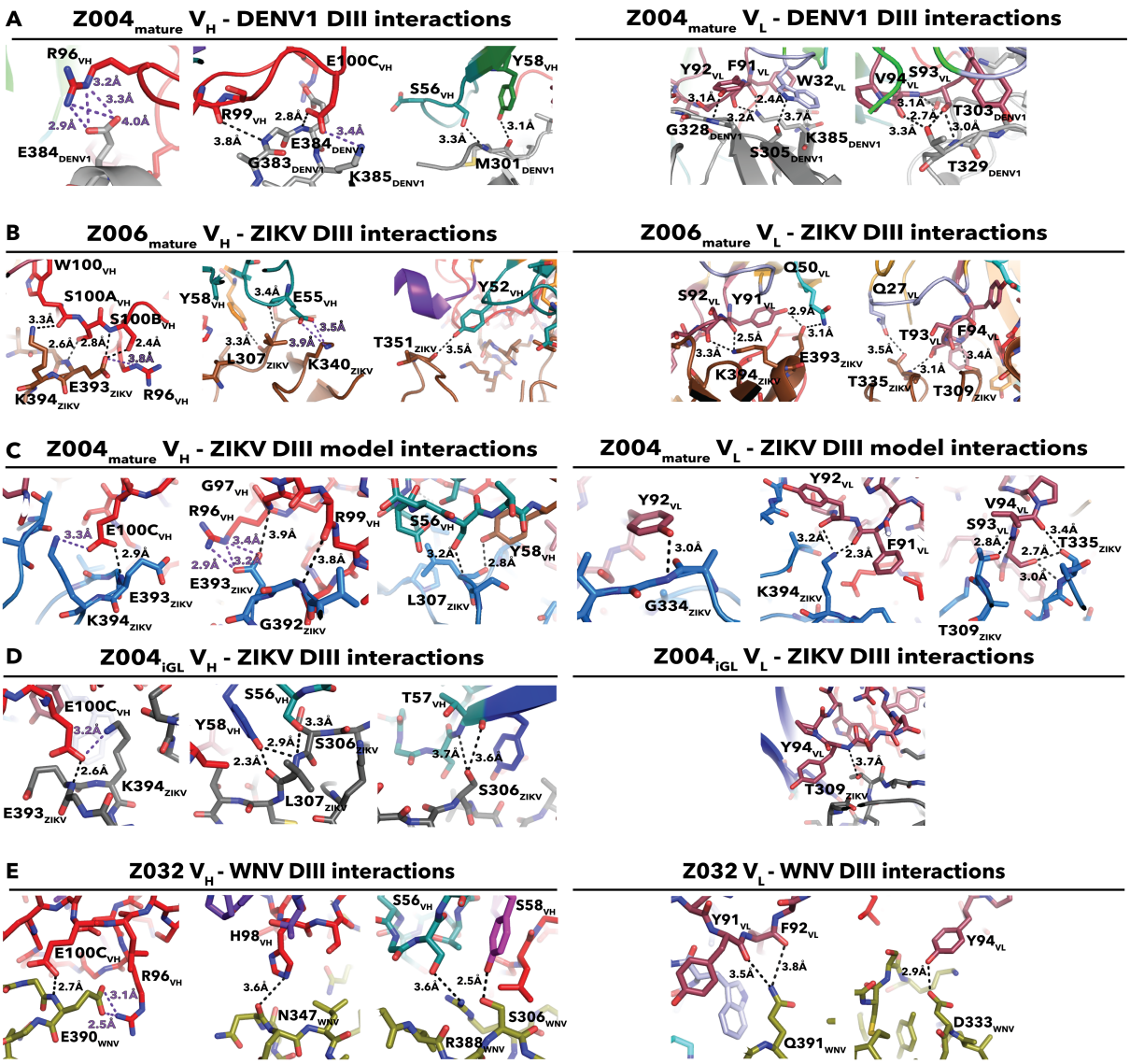

Figure S16. Close-up view of Fab–EDIII interactions. Interactions with V_H are shown on the left and interactions with V_L are shown on the right. **A.** $Z004_{mature}$–DENV1 EDIII crystal structure (PDB 5VIC). **B.** $Z006_{mature}$–ZIKV EDIII crystal structure (PDB 5VIG). **C.** $Z004_{mature}$–ZIKV EDIII homology model. **D.** $Z004_{iGL}$–ZIKV EDIII crystal structure (PDB 6UTA). **E.** $Z032_{mature}$–WNV EDIII crystal structure (PDB 6UTE).

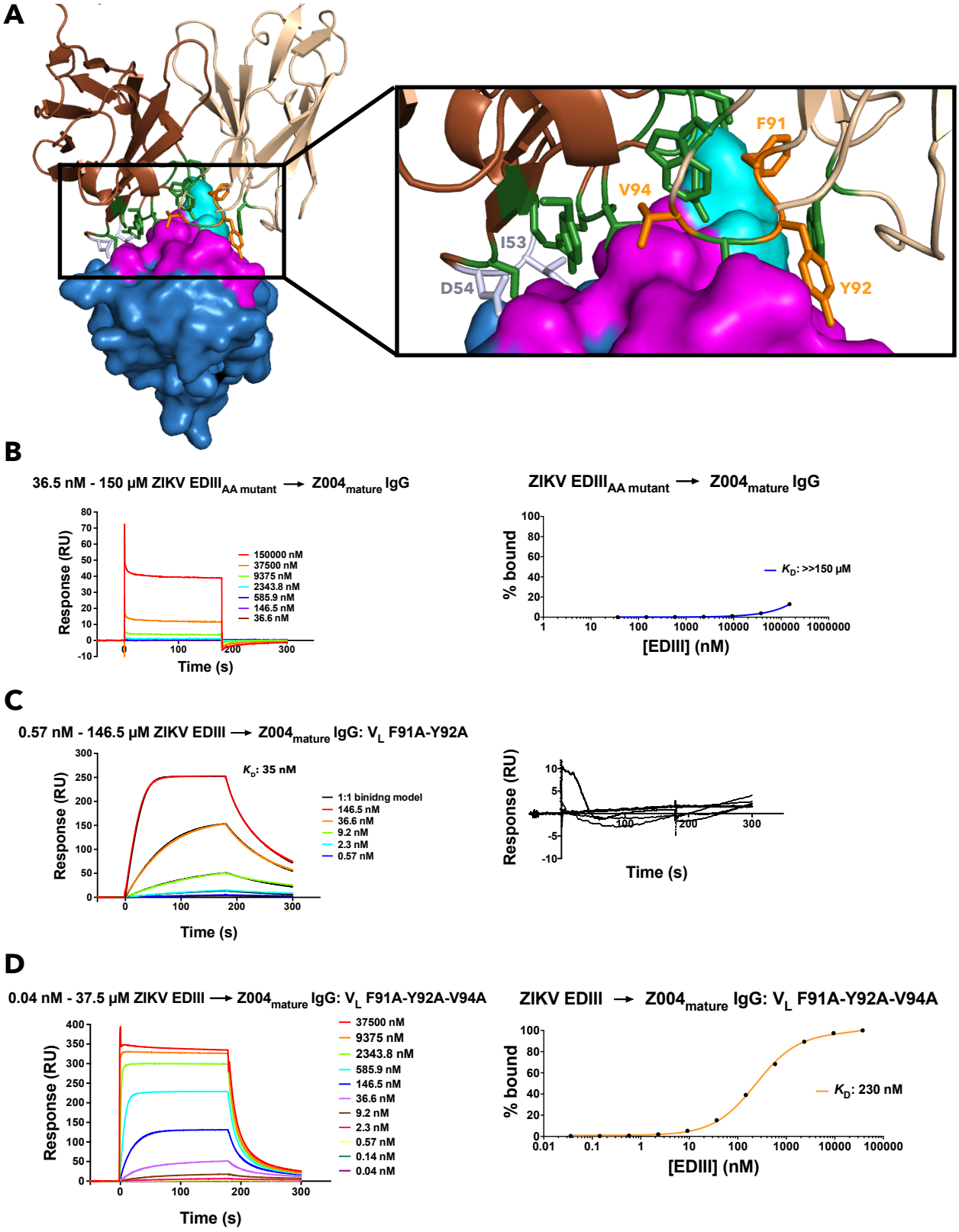

Figure S17. Comparison of ZIKV EDIII binding to Z004$_{mature}$ IgGs with site-directed mutations in the V_L. **A.** Z004$_{mature}$ V_HV_L–ZIKV EDIII homology model showing residues that differ between iGL

and mature Z004 Fab at the EDIII-binding interface. $Z004_{mature}$ V_HV_L (dark brown, V_H; tan, V_L) is shown as a cartoon representation and ZIKV EDIII (dark blue) is shown as a surface representation. EDIII residues within 4 Å of the V_HV_L are shown in magenta with the EK motif in teal. V_HV_L residues within 4 Å of the EDIII are shown in dark green with the V_H residues that differ between $Z004_{iGL}$ and $Z004_{mature}$ (but do not interact with EDIII), I53 and D54, shown in light purple and the V_L residues that differ between $Z004_{iGL}$ and $Z004_{mature}$ (and interact with EDIII), F91, Y92, and V94, shown in orange. **B-D.** SPR binding assays. IgGs were captured on a protein A biosensor chip, and the indicated concentrations of EDIII were injected. Sensorgrams are indicated in colors representing different injected concentrations. Y-axes show response units (RU). Five to 11 independent injections were performed. **B.** ZIKV $EDIII_{AA\ mutant}$ (E393A-K394A) binding to $Z004_{mature}$ IgG. **C-D.** ZIKV EDIII binding to $Z004_{mature}$ IgGs with alanine mutations in the V_L: F91A-Y92A (C) and F91A-Y92A-V94A (D). **C.** Fits to a 1:1 binding model are in black; since the model fits very closely fit the data, the models are only slightly visible. The corresponding residual plot is also shown. **B,D.** Normalized equilibrium binding response (R_{eq}) from the sensorgram is plotted versus the log of the concentration of the indicated injected proteins with the best fit binding curve to the experimental data points shown as a continuous line. The standard error of the fit for the 230 nM K_D was 12 nM, with a 95% confidence of 200-260 nM for ZIKV EDIII → $Z004_{mature}$ IgG: V_L F91A-Y92A-V94A. Since the ZIKV EDIII → $Z004_{mature}$ IgG binding reaction did not reach equilibrium, the K_D is approximated as greater than the highest concentration of analyte injected.

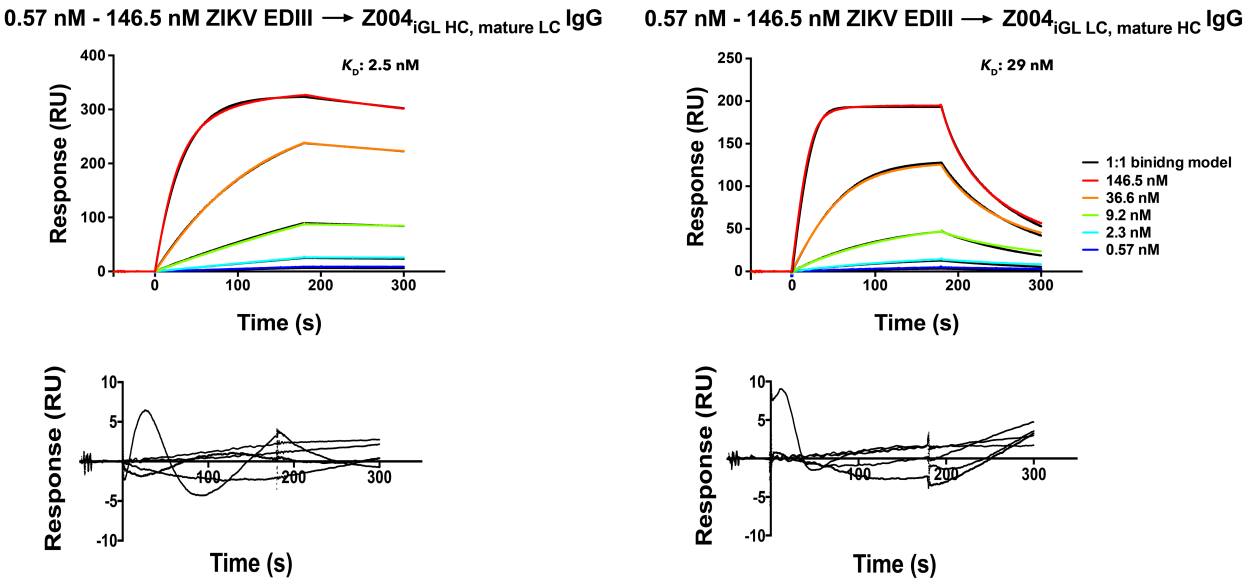

Figure S18. SPR binding sensorgrams (top; colored traces) and residual plots (bottom) for binding model fittings (top, black lines) of Z004 mature-iGL IgG chimeras (ligand) interacting with ZIKV EDIII (analyte). IgGs were captured on a protein A biosensor chip, and the indicated concentrations of ZIKV EDIII were injected. Sensorgrams are shown in colors representing different injected concentrations. Y-axes show response units (RU). Two independent experiments were performed.

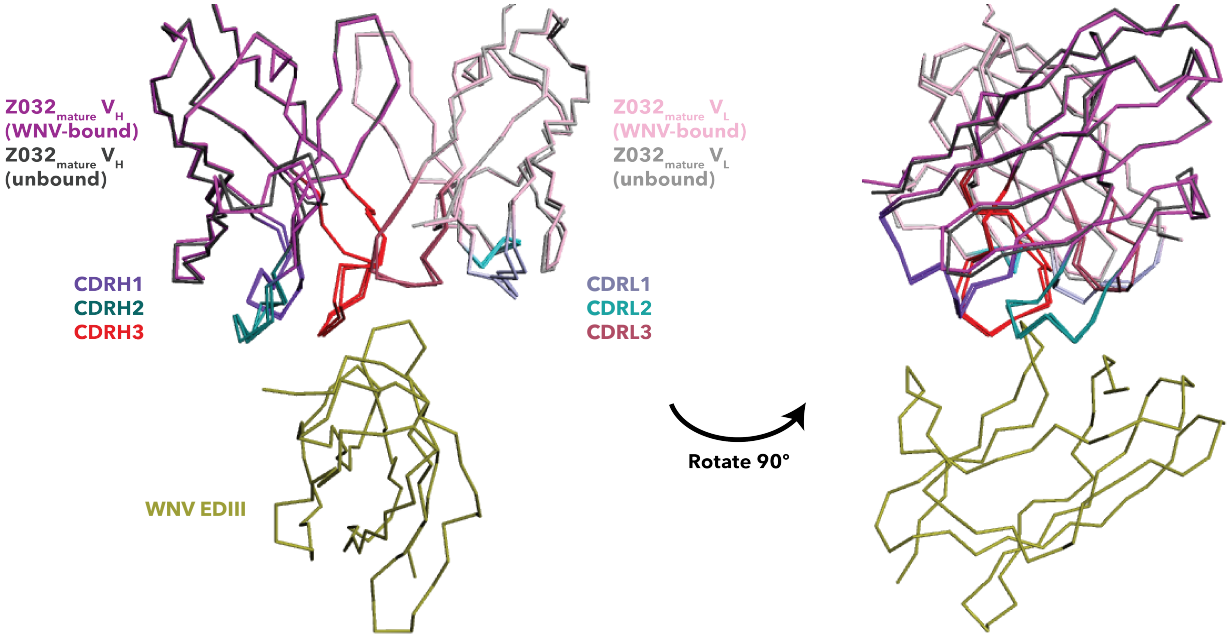

Figure S19. Comparison of bound and unbound structures of $Z032_{mature}$. **A.** Superimposition of V_H-V_L domains from the structure determination of a $Z032_{mature}$ Fab–WNV EDIII complex, in which the crystallographic asymmetric unit contained both bound (chains C and D) and unbound (chains E and F shown here) Fabs.

Table S1. X-ray diffraction data and refinement statistics for Fab-EDIII crystal structures.		
	Z004$_{iGL}$ Fab–ZIKV EDIII PDB 6UTA	**Z032$_{mature}$ Fab–WNV EDIII** PDB 6UTE
Data collection		
Space group	$P4_32_12$	$P2_1$
Cell dimensions		
a, *b*, *c* (Å)	85.91, 85.91, 327.46	96.23, 114.02, 127.26
α, β, γ (°)	90, 90, 90	90, 109.5, 90
Resolution (Å)	38.4-3.1	40.0-2.9
R_{pim} (%)	8.8 (49.1) *	9.5 (50.4)
$I / \sigma(I)$	9.1 (1.7)	5.6 (1.5)
Completeness (%)	93.6 (71.4)	99.7 (99.5)
Redundancy	12.4 (7.5)	3.1 (3.1)
CC(1/2)	0.99 (0.76)	0.98 (0.64)
Refinement		
Resolution (Å)	38.4-3.1	39.9-2.9
No. reflections	21817 (1618)	57390 (5694)
R_{work}/ R_{free}	27.4/29.3	22.3/26.5
No. atoms		
Peptide	8060	17255
Ligand	0	30
Water	0	0
B-factors		
Peptide	62.8	58.4
Ligand	0	80.1
Water	0	0
R.M.S. deviations		
Bond lengths (Å)	0.013	0.002
Bond angles (°)	1.56	0.55
Ramachandran statistics		
Ramachandran favored (%)	90.4	95.9
Ramachandran allowed (%)	7.54	3.97
Ramachandran outliers (%)	2.10	0.18
Number of TLS Groups	6	11

Each structure was derived from a single crystal.
*Highest resolution shell statistics shown in parentheses.

Table S2. Interacting residues in mature and iGL Fab–EDIII complexes*.

	V_H residues that interact with EDIII	V_L residues that interact with EDIII	EDIII residues that interact with Fab
$Z004_{iGL}$ Fab – ZIKV EDIII	$S56_{VH}$ (CDRH2) $T57_{VH}$ (CDRH2) $Y58_{VH}$ (FWRH3) $E100C_{VH}$ (CDRH3)	$Y94_{VL}$ (CDRL3)	$S306_{ZIKV}$ $L307_{ZIKV}$ $T309_{ZIKV}$ $E393_{ZIKV}$ $K394_{ZIKV}$
$Z004_{mature}$ Fab – ZIKV EDIII (homology model)	$S56_{VH}$ (CDRH2) $Y58_{VH}$ (FWRH3) $R96_{VH}$ (CDRH3) $G97_{VH}$ (CDRH3) $R99_{VH}$ (CDRH3) $E100C_{VH}$ (CDRH3)	$F91_{VL}$ (CDRL3) $Y92_{VL}$ (CDRL3) $S93_{VL}$ (CDRL3) $V94_{VL}$ (CDRL3)	$L307_{ZIKV}$ $T309_{ZIKV}$ $G334_{ZIKV}$ $T335_{ZIKV}$ $G392_{ZIKV}$ $E393_{ZIKV}$ $K394_{ZIKV}$
$Z004_{mature}$ Fab – DENV1 EDIII	$S56_{VH}$ (CDRH2) $Y58_{VH}$ (FWRH3) $R96_{VH}$ (CDRH3) $R99_{VH}$ (CDRH3) $E100C_{VH}$ (CDRH3)	$W32_{VL}$ (CDRL1) $F91_{VL}$ (CDRL3) $Y92_{VL}$ (CDRL3) $S93_{VL}$ (CDRL3) $V94_{VL}$ (CDRL3)	$M301_{DENV1}$ $T303_{DENV1}$ $S305_{DENV1}$ $G328_{DENV1}$ $T329_{DENV1}$ $G383_{DENV1}$ $E384_{DENV1}$ $K385_{DENV1}$
$Z006_{mature}$ Fab – ZIKV EDIII	$Y52_{VH}$ (CDRH2) $E55_{VH}$ (CDRH2) $Y58_{VH}$ (FWRH3) $R96_{VH}$ (CDRH3) $W100_{VH}$ (CDRH3) $S100A_{VH}$ (CDRH3) $S100B_{VH}$ (CDRH3)	$Q27_{VL}$ (CDRL1) $Q50_{VL}$ (CDRL2) $Y91_{VL}$ (CDRL3) $S92_{VL}$ (CDRL3) $T93_{VL}$ (CDRL3) $F94_{VL}$ (CDRL3)	$L307_{ZIKV}$ $T309_{ZIKV}$ $T335_{ZIKV}$ $K340_{ZIKV}$ $T351_{ZIKV}$ $E393_{ZIKV}$ $K394_{ZIKV}$
$Z032_{mature}$ Fab – WNV EDIII	$S56_{VH}$ (CDRH2) $Y58_{VH}$ (FWR3) $R96_{VH}$ (CDRH3) $H98_{VH}$ (CDRH3) $E100C_{VH}$ (CDRH3)	$Y91_{VL}$ (CDRL3) $F92_{VL}$ (CDRL3) $Y94_{VL}$ (CDRL3)	$S306_{WNV}$ $D333_{WNV}$ $N347_{WNV}$ $R388_{WNV}$ $E390_{WNV}$ $Q391_{WNV}$

*The Kabat numbering scheme was used.

Table S3. K_Ds (nM) of Z004 Ab (mature, iGL, chimeras, and mutants) binding to ZIKV EDIII determined by SPR.

IgG	EDIII	K_D (nM)
Z004$_{mature}$	ZIKV	0.28
Z004$_{iGL}$	ZIKV	1200
Z004$_{iGL\ LC,\ mature\ HC}$	ZIKV	29
Z004$_{iGL\ HC,\ mature\ LC}$	ZIKV	2.5
Z004$_{mature}$	ZIKV$_{AA\ mutant}$	>>150 μM
Z004$_{mature}$: V_L F91A-Y92A	ZIKV	35
Z004$_{mature}$: V_L F91A-Y92A-V94A	ZIKV	230

Table S4. Pairwise superimpositions and rmsd calculations of bound and unbound V_HV_L chains in the $Z032_{mature}$–WNV EDIII crystal structure.

$Z032_{mature}$ V_HV_L chains: Set 1	**$Z032_{mature}$ V_HV_L chains: Set 2**	**Cα atom count**	**rmsd (Å)**
C and D (bound)	A and B (unbound)	213	0.42
C and D (bound)	E and F (unbound)	210	0.45
C and D (bound)	G and H (unbound)	217	0.35
C and D (bound)	I and J (unbound)	211	0.42
A and B (unbound)	E and F (unbound)	203	0.22
A and B (unbound)	G and H (unbound)	204	0.32
A and B (unbound)	I and J (unbound)	206	0.39
E and F (unbound)	G and H (unbound)	210	0.37
E and F (unbound)	I and J (unbound)	212	0.47
G and H (unbound)	I and J (unbound)	214	0.41

References

1. Robbiani, D. F. *et al.* Recurrent Potent Human Neutralizing Antibodies to Zika Virus in Brazil and Mexico. *Cell* **169**, 597-609.e11 (2017).